

Enormous Fluid Antenna Systems (E-FAS) for Multiuser MIMO: Channel Modeling and Analysis

Farshad Rostami Ghadi, *Member, IEEE*, Kai-Kit Wong, *Fellow, IEEE*,
 Masoud Kaveh, *Member, IEEE*, Wee Kiat New, *Member, IEEE*, Chan-Byoung Chae, *Fellow, IEEE*,
 and Lajos Hanzo, *Life Fellow, IEEE*

Abstract—Enormous fluid antenna systems (E-FAS), the system concept that utilizes position reconfigurability in the large scale, have emerged as a new architectural paradigm where intelligent surfaces are repurposed from passive smart reflectors into multi-functional electromagnetic (EM) interfaces that can route guided surface waves over walls, ceilings, and building facades, as well as emit space waves to target receivers. This expanded functionality introduces a new mode of signal propagation, enabling new forms of wireless communication. In this paper, we provide an analytical performance characterization of an E-FAS-enabled wireless link. We first develop a physics-consistent end-to-end channel model that couples a surface-impedance wave formulation with small-scale fading on both the base station (BS)-surface and launcher-user segments. We illustrate that the resulting effective BS-user channel remains circularly symmetric complex Gaussian, with an enhanced average power that explicitly captures surface-wave attenuation and junction losses. For single-user cases with linear precoding, we derive the outage probability and ergodic capacity in closed forms, together with high signal-to-noise ratio (SNR) asymptotics that quantify the gain of E-FAS over purely space-wave propagation. For the multiuser case with zero-forcing (ZF) precoding, we derive the distribution of the signal-to-interference-plus-noise ratio (SINR) and obtain tractable approximations for the ergodic sum-rate, explicitly revealing how the E-FAS macro-gain interacts with the BS spatial degrees of freedom (DoF). In summary, our analysis shows that E-FAS preserves the diversity order dictated by small-scale fading while improving the coding gain enabled by cylindrical surface-wave propagation.

Index Terms—Fluid antenna system (FAS), surface wave communication, multiuser MIMO, shadowing.

The work of F. Rostami Ghadi, K. K. Wong, and W. K. New is supported by the Engineering and Physical Sciences Research Council (EPSRC) under Grant EP/W026813/1.

The work of C.-B. Chae is supported by the Institute for Information and Communication Technology Planning and Evaluation (IITP)/National Research Foundation of Korea (NRF) grant funded by the Ministry of Science and ICT (MSIT), South Korea, under Grant RS-2024-00428780 and 2022R1A5A1027646.

The work of L. Hanzo is supported by the Engineering and Physical Sciences Research Council (EPSRC) projects Platform for Driving Ultimate Connectivity (TITAN) under Grant EP/X04047X/1 and Grant EP/Y037243/1.

F. Rostami Ghadi, K. K. Wong, and W. K. New are with the Department of Electronic and Electrical Engineering, University College London, WC1E 7JE London, United Kingdom. K. K. Wong is also affiliated with Yonsei Frontier Lab., Yonsei University, Seoul, Republic of Korea (e-mail: {f.rostamighadi, kai-kit.wong}@ucl.ac.uk, aven.wknew@yahoo.com).

M. Kaveh is with the Department of Information and Communication Engineering, Aalto University, Espoo, Finland. (e-mail: masoud.kaveh@aalto.fi).

C.-B. Chae is with the School of Integrated Technology, Yonsei University, Seoul, 03722, Republic of Korea (e-mail: cbchae@yonsei.ac.kr).

L. Hanzo is with the School of Electronics and Computer Science, University of Southampton, Southampton, United Kingdom (e-mail: lh@ecs.soton.ac.uk).

Corresponding Author: Kai-Kit Wong.

I. INTRODUCTION

A. Background

THE EVER-GROWING demand of network capacity, the more ambitious targets on various key performance indicators (KPIs) and the constant push by emerging services such as augmented or extended reality, holographic communication, and internet-of-things (IoT), etc., continue to put pressure on existing mobile communication technologies, heading towards the sixth generation (6G) [1], [2], [3]. Current physical layer has been relying on multiuser multiple-input multiple-output (MU-MIMO) to provide the needed capacity [4]. As a matter of fact, since the pioneering work by Foschini [5] and Telatar [6] in the late 90s, MIMO has become a principal technology in the physical layer. MIMO then evolved into MU-MIMO in the fourth generation (4G) [7], [8], [9], [10], [11], becoming so powerful that saw it to scale up in the massive version in the fifth generation (5G) [12], [13], from 8 antennas in 4G to 64 antennas in 5G at the base station (BS).

Looking to delivering 6G, there has been strong interest to deploy even more antennas at the BS [14] and migrate toward higher carrier frequencies [15]. However, the latter increases the vulnerability of wireless links due to blockage, penetration loss, and unfavorable propagation conditions [16]. It is worth noting that the MU-MIMO precoding with a larger array will increase the peak-to-average power ratio (PAPR) even more, which greatly degrades the efficiency of power amplifiers and increases the power consumption. With blockage in the high frequency bands, there is a legitimate concern that the power consumption of the BS cannot keep up and the communication performance would be considerably limited, especially when the line-of-sight (LoS) is obstructed, and where conventional space wave transmission suffers from severe path loss due to spherical wave spreading and few diffraction capabilities [17].

To tackle this, reconfigurable intelligent surfaces (RIS), e.g., [18], [19], [20], [21], and their extensions such as simultaneous transmitting and reflecting RIS (STAR-RIS) [22], have been widely investigated in recent years, as a means of reshaping the wireless propagation environment by programmable phase and amplitude control on the incident electromagnetic (EM) waves for ‘smart’ reflections. Though these architectures can redirect or partially forward energy toward desired locations, their operations are fundamentally based on three-dimensional (3D) space wave propagation. Therefore, the achievable performance gains are still constrained by spherical power decay and, in many situations, by the doubly fading and path loss

effects as well. Additionally, the reliance on fine-grained EM control and accurate channel state information (CSI) across large surfaces introduces severe system complexity, particularly in dense multiuser deployments [23].

While MU-MIMO systems should continue to dominate the physical layer for years to come, it is evident that we need other technologies to assist and complement MU-MIMO. In other words, we should seek to enhance its capability without the need of increasing the number of antennas. On the other hand, although it is widely accepted that RIS can be deployed to create a more favorable environment for communication, the reality is that RISs are too complex and expensive to operate. The indication is that existing RIS technologies are not ready to be included in the 6G cycle until further breakthroughs.

B. Reconfigurable Antenna-aided Communications

One possible technology to elevate MIMO is the adoption of reconfigurable antennas [24] and the first effort dates back to early 2000s by Cetiner *et al.* in [25]. However, fast forward to today, reconfigurable antennas are still yet to revolutionize wireless communication technologies. This stems from a gap between existing reconfigurable antenna capabilities and the capabilities needed to transform wireless communications. To address this, Wong *et al.* introduced the fluid antenna system (FAS) [26], [27] which is a hardware-agnostic system concept that considers the antenna as a reconfigurable physical-layer resource to broaden system design and network optimization, and inspire next-generation reconfigurable antennas [28], [29], [30], [31], [32]. Basically, FAS represents all forms of reconfigurable antenna-aided wireless communications systems. In practice, FAS may be implemented by movable elements [33], liquid-based antennas [34], [35], metamaterial-based antennas [36], [37], [38], reconfigurable pixels [39], [40], [41], etc. In [42], Tong *et al.* compared various FAS prototypes.

After the seminal work in [26], [27], numerous researches have emerged to understand the diversity benefits of antenna position reconfigurability. For instance, in [43], an analytical approximation was proposed to handle the correlation among FAS ports. Copula techniques have also been applied to study the performance of FAS under arbitrary fading channels [44]. The diversity order for the FAS channel under Rayleigh fading was characterized in [45]. A particular difficulty in analyzing FAS is the need to address the spatial correlation. To tackle this issue, [46] introduced the spatial block-correlation model that can keep the analysis tractable while preserving accuracy. In [47], FAS was considered at both ends, giving rise to the MIMO-FAS channel and it was illustrated that extraordinary diversity gains can be obtained over the fixed MIMO system. Moreover, continuous FAS was also studied recently in [48]. Besides single-user systems, FAS can also combine MIMO as an additional degree of freedom (DoF) to enhance multiuser communications, see e.g., [49], [50]. CSI is important to the effective operation of FAS. Recently, this was investigated by exploiting channel sparsity [51], learning-based methods [52], Nyquist sampling and maximum likelihood estimation [53], and successive Bayesian reconstruction [54].

Another line of research sees FAS synergize RIS-assisted communications. One direction is to consider the use of FAS

at the mobile user receiver in a RIS-aided channel [55], [56], [57]. More interestingly, the FAS concept can be applied to empower each element of RIS with position reconfigurability. This has led to the fluid RIS (FRIS) system [58], [59], [60], [61]. It is also possible to apply the FAS approach into STAR-RIS, giving rise to the fluid integrated reflecting and emitting surfaces (FIRES) [62]. These approaches extend the concept of fluid antennas from point-like elements to metasurface-based structures, enabling the dynamic reconfiguration of reflecting and radiating elements across a surface. While both FRIS and FIRES offer additional flexibility in shaping the radiation and reflection characteristics of the surface, they remain inherently power-inefficient because space wave spreads over 3D space and sophisticated signal processing needs to be done to form focused beams towards the target receivers.

To fundamentally address the limitations of wireless communication, [63] proposed a new paradigm in which intelligent surfaces are leveraged not only as emitters, but as engineered propagation media. Such surface-confined propagation dramatically reduces path-loss, thereby improving power efficiency, and limits unintended radiation, hence mitigating over-the-air interference. Additionally, since signal behavior is largely dictated by surface geometry, interference management becomes much more predictable, while the guided nature of propagation enables highly reliable links that closely resemble persistent LoS conditions [64], [65], [66]. This paradigm was recently referred to as an enormous FAS (E-FAS) in [67]. Specifically, an ensemble of intelligent surfaces each capable of acting as surface-wave propagation media for routing and emitters for signal transmission, is interpreted as an enormous version of FAS, exploiting position reconfigurability in the large scale. E-FAS departs fundamentally from conventional approaches by shifting the focus from antenna or surface reconfiguration to propagation reconfiguration. Rather than treating intelligent surfaces as passive reflectors, E-FAS reimagines surfaces as guided EM interfaces that convert incident space waves into surface waves and vice versa. These surface waves propagate along engineered surfaces with cylindrical spreading, leading to substantially reduced attenuation compared to conventional space wave 3D propagation. By routing energy along walls, ceilings, or building exteriors and radiating only in the final hop, E-FAS enables LoS-like connectivity even in shadowed environments, greatly improving power efficiency.

C. Motivation and Contributions

Despite the attractive propagation advantages envisaged by E-FAS, its performance is not well understood, with only a few results based on computer simulations for signal-to-noise ratio (SNR). A fundamental understanding of how surface wave-assisted propagation translates into classical communication-theoretic performance metrics is missing. Moreover, there is no analytical characterization of the effective end-to-end channel statistics induced by E-FAS, nor of its KPIs such as outage probability, ergodic capacity, and sum-rate under MU-MIMO precoding. Different from [67], this paper provides the first closed-form, end-to-end statistical characterization of E-FAS-aided channels and their impact on communication-theoretic

metrics. The results allow rigorous benchmarking, scalability analysis, and system-level insights that are not accessible via EM simulations alone. In particular, our objective is to develop a tractable self-contained performance analysis framework for E-FAS-aided wireless systems from an information-theoretic perspective, and bridge the E-FAS model with established tools in random matrix theory and wireless performance analysis. The distinctive contributions of our work, compared to the literature, are highlighted in Table I. Technically speaking, our contributions are summarized as follows:

- Equivalent channel modeling—We reformulate the original E-FAS signal model into a compact end-to-end channel representation that captures the combined effect of surface wave-assisted propagation and small-scale fading. Under justifiable assumptions, we show that the resulting equivalent BS-user equipment (UE) channel follows a complex Gaussian distribution with an enhanced average power that reflects cylindrical surface wave attenuation.
- Single-user performance analysis—For single-user transmission with linear transmit precoding, we derive closed-form expressions for the outage probability and ergodic capacity. High-SNR asymptotic analysis reveals that E-FAS provides a power gain, while preserving the diversity order of the underlying fading channel.
- Multiuser zeroforcing (ZF) analysis—For the downlink, we analyze ZF precoding and characterize the distribution of the post-processing signal-to-interference-plus-noise ratio (SINR). Based on this characterization, we derive accurate approximations for the ergodic sum-rate that capture the impact of the E-FAS on the channel gain and the excess spatial DoF available at the transmitter.
- Benchmarking and validation—A baseline without E-FAS is considered by fixing the direct link large-scale gain, facilitating fair and physically meaningful performance comparisons that isolate the impact of surface wave-assisted propagation. Extensive Monte-Carlo simulations are used to validate all analytical results, and our findings demonstrate that E-FAS yields substantial gains in outage performance, ergodic capacity, and multiuser spectral efficiency under practical system parameters.

D. Organization and Notations

The remainder of this paper is organized as follows. Section II introduces the system and channel model. Section III derives the equivalent end-to-end channel distribution of E-FAS-assisted propagation. Then Sections IV and V analyze the single-user and multiuser transmission scenarios, respectively. Our numerical results are presented in Section VI, and concluding remarks are given in Section VII.

Notations—Scalars, vectors, and matrices are denoted by lowercase letters, bold lowercase letters, and bold uppercase letters, respectively. The operators $(\cdot)^T$, $(\cdot)^H$, and $\text{tr}(\cdot)$ denote transpose, Hermitian transpose, and trace. The expectation operator is denoted by $\mathbb{E}\{\cdot\}$. The notation $\mathcal{CN}(\mu, \mathbf{C})$ represents a circularly symmetric complex Gaussian distribution with mean μ and covariance matrix \mathbf{C} . The identity matrix of appropriate dimension is denoted by \mathbf{I} . The Euclidean norm is denoted by

$\|\cdot\|$. Unless otherwise stated, $\log(\cdot)$ and $\log_2(\cdot)$ denote the natural and base-2 logarithms, respectively. The main symbols and variables used throughout are summarized in Table II.

II. SYSTEM AND CHANNEL MODEL

Consider the downlink system as shown in Fig. 1, in which an M -antenna BS communicates with K single-antenna UEs in an environment equipped with an E-FAS. The E-FAS comprises distributed metasurface tiles mounted on surrounding structures. These tiles convert incident space waves into guided surface waves that propagate along engineered pathways and are eventually re-radiated toward the intended UEs through programmable launchers [68, Section III]. This layered propagation structure yields a composite channel formed by

- A BS-to-surface excitation segment,
- A deterministic surface wave propagation stage,
- A launcher interface, and
- A final space wave hop to each UE.

A. Transmit Signal Model

For the model considered, let $x_u \in \mathbb{C}$ denote the data symbol intended for UE u , normalized such that $\mathbb{E}\{|x_u|^2\} = 1$. The BS applies a linear precoding $\mathbf{w}_u \in \mathbb{C}^M$ to this symbol, resulting in the transmit vector

$$\mathbf{x} = \sum_{u=1}^K \sqrt{P_u} \mathbf{w}_u x_u, \quad (1)$$

where P_u is the power allocated to UE u and $\sum_{u=1}^K P_u = P$ is the power budget of the BS. Unless otherwise stated, $P_u = P/K, \forall u$, is adopted for analytical clarity.

B. BS-to-Surface Excitation

The signal emitted by the BS illuminates the metasurface tiles and excites the guided-wave interface. The channel between the BS array and the N_s effective excitation ports is denoted by $\mathbf{H}_{\text{BS-sur}} \in \mathbb{C}^{N_s \times M}$. For tractability, and following a common assumption in analytical studies, this segment is modeled by Rayleigh fading with large-scale gain β_{BS} , i.e.,

$$\mathbf{H}_{\text{BS-sur}} = \sqrt{\beta_{\text{BS}}} \mathbf{G}_{\text{BS-sur}}, \quad (2)$$

in which $\mathbf{G}_{\text{BS-sur}}$ contains independent and identically distributed (i.i.d.) $\mathcal{CN}(0, 1)$ entries.

C. Surface Wave Propagation

Once excited, the EM field propagates along the metasurface as a guided surface wave. For a propagation distance d along the engineered path, the surface wave envelope is given by

$$H_{\text{sw}}(d) = A_0 e^{-\alpha d} e^{-j\beta d}, \quad (3)$$

where A_0 incorporates both coupling and the excitation efficiency related to local impedance matching, in which $\alpha = \Re\{\gamma\}$ and $\beta = \Im\{\gamma\}$ represent the attenuation and phase constants, respectively. The surface wave propagation constant γ is governed by the surface impedance Z_{sur} through

$$\gamma = \sqrt{-\omega^2 \mu_0 \varepsilon_0 - (-j\omega \varepsilon_0 Z_{\text{sur}})^2}, \quad (4)$$

TABLE I
CONTRASTING OUR CONTRIBUTIONS TO THE EXISTING LITERATURE.

Features	[67]	[63]	[64]	[65]	[66]	[58]	[60]	[62]	This paper
E-FAS	✓								✓
Cylindrical surface wave propagation	✓	✓	✓	✓	✓				✓
Environment-embedded reconfigurable surfaces	✓	✓	✓	✓	✓	✓	✓	✓	✓
Geometrically reconfigurable radiating aperture	✓	✓	✓	✓	✓	✓	✓	✓	✓
Statistical channel modeling							✓		✓
Outage probability							✓		✓
Sum-rate/ergodic rate						✓	✓	✓	✓

TABLE II
SUMMARY OF MAIN NOTATIONS

Symbol	Description
M	Number of antennas at the BS
K	Number of UEs
\mathbf{x}	Transmit signal vector at the BS
x_u	Information symbol intended for UE u
P	Total BS transmit power
P_u	Transmit power allocated to UE u
\mathbf{w}_u	Precoding vector for UE u
$\mathbf{H}_{\text{BS-sur}}$	BS-to-surface space wave channel matrix
\mathbf{H}_{sur}	Surface wave propagation channel
$\mathbf{W}_{\text{relay}}$	Surface launcher / relay processing matrix
$\mathbf{h}_{\text{relay-UE},u}$	Launcher-to-UE channel vector
$h_{u,q}^{\text{dl}}$	Direct BS-to-UE channel coefficient
\mathbf{h}_u^{eq}	Equivalent end-to-end BS-to-UE channel vector
h_u^{eq}	Effective channel for UE u
β_{DL}	Large-scale gain of the direct BS-to-UE link
Ω_{sw}	Surface wave-assisted channel gain
Ω_{eq}	Equivalent end-to-end channel variance
σ^2	Thermal noise variance at the UE
σ_{eff}^2	Effective noise variance including relay noise
γ_u	Instantaneous received SINR at UE u
γ_u^{ZF}	Post-ZF SINR for UE u
ρ	Average SNR parameter
\mathbf{H}_{eq}	Equivalent BS-to-UE channel matrix
\mathbf{G}	Gram matrix $\mathbf{H}_{\text{eq}}^H \mathbf{H}_{\text{eq}}$
m	ZF diversity parameter
R_0	Target transmission rate
P_{out}	Outage probability
C	Ergodic capacity
$R_{\text{sum}}^{\text{ZF}}$	ZF ergodic sum-rate

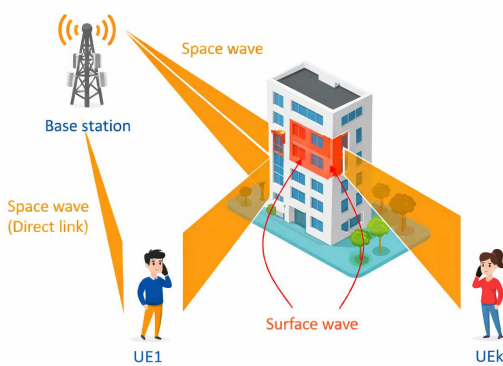


Fig. 1. A downlink E-FAS-aided environment model with an M -antenna BS communicating to K single-antenna UEs.

with ω being the operating angular frequency and (μ_0, ε_0) the free-space permeability and permittivity [67].

Therefore, the full surface wave channel is formulated as

$$\mathbf{H}_{\text{sur}} = H_{\text{sw}}(d) \mathbf{G}_{\text{path}}, \quad (5)$$

where $\mathbf{G}_{\text{path}} \in \mathbb{C}^{N_s \times N_s}$ is a deterministic routing matrix that specifies the activated tiles and junctions forming the guided pathway. Hence, \mathbf{H}_{sur} is treated as deterministic for a fixed geometric configuration [67], reflecting the guided and engineered nature of surface wave propagation in E-FAS.¹

D. Launcher Processing and Noise

At the termination of the guided path (that should be made close to the intended UEs), programmable launchers reconvert the surface wave into a space wave directed toward the UEs. Their operation is represented by a relay processing matrix $\mathbf{W}_{\text{relay}} \in \mathbb{C}^{N_L \times N_s}$ with N_L launcher ports as

$$\mathbf{W}_{\text{relay}} = \alpha_r \mathbf{U}, \quad (6)$$

where α_r denotes a complex amplification factor and \mathbf{U} is a unitary or selection matrix. The relay electronics introduce thermal noise $\mathbf{n}_{\text{relay}} \sim \mathcal{CN}(\mathbf{0}, \sigma_r^2 \mathbf{I}_{N_s})$, which

$$z_{u,\text{relay}} = \mathbf{h}_{\text{relay-UE},u} \mathbf{W}_{\text{relay}} \mathbf{n}_{\text{relay}}, \quad (7)$$

to the received signal at the u -th UE.

E. Launcher-to-UE and Direct BS-to-UE Channels

The final hop from the launchers to UE u is characterized by

$$\mathbf{h}_{\text{relay-UE},u} = \sqrt{\beta_{\text{LU},u}} \mathbf{g}_{\text{relay-UE},u}, \quad (8)$$

where $\mathbf{g}_{\text{relay-UE},u}$ contains i.i.d. $\mathcal{CN}(0, 1)$ entries, and $\beta_{\text{LU},u}$ denotes the associated large-scale gain.

In addition, the BS may have a residual direct path to UE u through penetration or partial blockage. Hence, this direct link is defined as

$$\mathbf{h}_u^{\text{dl}} = \sqrt{\beta_{\text{DL},u}} \mathbf{g}_u^{\text{dl}}, \quad (9)$$

with $\mathbf{g}_u^{\text{dl}} \in \mathbb{C}^{1 \times M}$ having i.i.d. $\mathcal{CN}(0, 1)$ entries and $\beta_{\text{DL},u}$ representing the large-scale attenuation. A fully blocked scenario corresponds to setting $\beta_{\text{DL},u} = 0$.

¹In line with the E-FAS framework, surface wave propagation is modeled as deterministic for a fixed metasurface configuration, reflecting its guided, impedance-controlled nature and the absence of rich multipath scattering. Random fading is therefore confined to the space wave segments before surface excitation and after re-radiation [67].

$$y_u = \sqrt{P_u} (\mathbf{h}_{\text{relay-UE},u} \mathbf{W}_{\text{relay}} \mathbf{H}_{\text{sur}} \mathbf{H}_{\text{BS-sur}} \mathbf{w}_u + \mathbf{h}_u^{\text{dl}} \mathbf{w}_u) x_u + \sum_{i \neq u} \sqrt{P_i} (\mathbf{h}_{\text{relay-UE},u} \mathbf{W}_{\text{relay}} \mathbf{H}_{\text{sur}} \mathbf{H}_{\text{BS-sur}} \mathbf{w}_i + \mathbf{h}_u^{\text{dl}} \mathbf{w}_i) x_i + z_{u,\text{relay}} + n_u \quad (11)$$

F. End-to-End Received Signal Model

Upon combining all the components, the signal received by UE u becomes

$$y_u = \mathbf{h}_{\text{relay-UE},u} \mathbf{W}_{\text{relay}} \mathbf{H}_{\text{sur}} \mathbf{H}_{\text{BS-sur}} \mathbf{x} + \mathbf{h}_u^{\text{dl}} \mathbf{x} + z_{u,\text{relay}} + n_u, \quad (10)$$

where $n_u \sim \mathcal{CN}(0, \sigma^2)$ denotes the receiver noise. Substituting $\mathbf{x} = \sum_{i=1}^K \sqrt{P_i} \mathbf{w}_i x_i$ into (10) gives (11) (see top of this page). The summation over $i \neq u$ in (11) represents the inter-user interference created by the signals intended for the remaining UEs. Upon defining the effective end-to-end channel coefficient associated with stream x_i as

$$h_{u,i}^{\text{eq}} \triangleq \mathbf{h}_{\text{relay-UE},u} \mathbf{W}_{\text{relay}} \mathbf{H}_{\text{sur}} \mathbf{H}_{\text{BS-sur}} \mathbf{w}_i + \mathbf{h}_u^{\text{dl}} \mathbf{w}_i, \quad (12)$$

the received signal finally becomes

$$y_u = \sqrt{P_u} h_{u,u}^{\text{eq}} x_u + \sum_{i \neq u} \sqrt{P_i} h_{u,i}^{\text{eq}} x_i + z_{u,\text{relay}} + n_u, \quad (13)$$

which is the complete multiuser E-FAS downlink model.

III. END-TO-END CHANNEL STATISTICS

The performance analysis in the following sections relies on the statistical characterization of the composite end-to-end channel experienced by each UE. In particular, outage probability and ergodic capacity expressions depend on the distribution of the effective scalar channel coefficient $h_{u,i}^{\text{eq}}$, which incorporates both the surface wave-assisted path and the direct BS-UE link. As \mathbf{H}_{sur} is deterministic for a given E-FAS configuration and routing geometry, the randomness in $h_{u,i}^{\text{eq}}$ arises entirely from small-scale fading on the BS-surface and launcher-UE segments as well as the distribution of the BS precoder. This section establishes the distribution of the equivalent channel under the assumptions that allow tractable performance analysis. We begin with the single-user case and later extend the insights to the multiuser case.

A. Scalar Effective Channel

For the user of interest, say UE u , the relevant effective channel is $h_u^{\text{eq}} \triangleq h_{u,u}^{\text{eq}}$, expressed as

$$h_u^{\text{eq}} = \underbrace{\mathbf{h}_{\text{relay-UE},u} \mathbf{W}_{\text{relay}} \mathbf{H}_{\text{sur}} \mathbf{H}_{\text{BS-sur}} \mathbf{w}_u}_{h_u^{\text{sw}}} + \underbrace{\mathbf{h}_u^{\text{dl}} \mathbf{w}_u}_{h_u^{\text{dl,eff}}}. \quad (14)$$

The first term represents propagation along the surface wave-guided E-FAS path, while the second term captures the effective projection of the direct BS-UE channel onto the liner precoding vector \mathbf{w}_u .

To derive closed-form distributions, we proceed with the single-user case ($K = 1$), where the structure is simplest and the essential stochastic behavior is most transparent.

B. Single-User Case and Precoder Model

In a single-user scenario, the optimal BS strategy under perfect channel knowledge would be maximum ratio transmission (MRT) with respect to the full composite channel. However, since the composite channel depends on both the surface wave routing and the intermediate propagation segments that may not be directly observable at the BS, a fully informed MRT having perfect end-to-end channel information may not be available. To capture this uncertainty while maintaining analytical tractability, we adopt the following standard assumption. In the single-user setting, we consider that the BS precoding \mathbf{w} is modelled as a unit-norm isotropically distributed random vector independent of $\mathbf{H}_{\text{BS-sur}}$ and $\mathbf{h}_{\text{relay-UE}}$, i.e.,

$$\mathbf{w} \sim \text{Unif}(\mathbb{S}^{M-1}), \quad (15)$$

in which $\|\mathbf{w}\| = 1$.

This abstraction reflects scenarios where the BS does not exploit CSI, or relies on long-term channel statistics or wide beams. Under this assumption, the effective channel becomes a projection of a Gaussian row vector onto a random unit-norm direction, enabling a clean analytical characterization.

C. Distribution of the Surface Wave-Assisted Component

Let the row vector \mathbf{T}_u which is defined as

$$\mathbf{T}_u \triangleq \mathbf{h}_{\text{relay-UE},u} \mathbf{W}_{\text{relay}} \mathbf{H}_{\text{sur}} \mathbf{H}_{\text{BS-sur}} \in \mathbb{C}^{1 \times M}, \quad (16)$$

so that $h_u^{\text{sw}} = \mathbf{T}_u \mathbf{w}$. As a consequence, we characterize its distribution as the following lemma.

Lemma 1. Define $\mathbf{H}_{\text{BS-sur}} = \sqrt{\beta_{\text{BS}}} \mathbf{G}_{\text{BS-sur}}$ with independent $\mathcal{CN}(0, 1)$ entries, and let $\mathbf{h}_{\text{relay-UE},u} = \sqrt{\beta_{\text{LU},u}} \mathbf{g}_{\text{relay-UE},u}$ with independent $\mathcal{CN}(0, 1)$ entries. Assume further that \mathbf{H}_{sur} and $\mathbf{W}_{\text{relay}}$ are deterministic. Then \mathbf{T}_u is a zero-mean complex Gaussian vector with covariance

$$\mathbb{E}\{\mathbf{T}_u^H \mathbf{T}_u\} = \Omega_{\text{sw},u} \mathbf{I}_M, \quad (17)$$

where

$$\Omega_{\text{sw},u} = \frac{\beta_{\text{BS}} \beta_{\text{LU},u}}{M} \text{tr}(\mathbf{H}_{\text{sur}}^H \mathbf{W}_{\text{relay}}^H \mathbf{W}_{\text{relay}} \mathbf{H}_{\text{sur}}). \quad (18)$$

Proof: By construction, \mathbf{T}_u can be written as a linear transformation of the Gaussian matrix $\mathbf{G}_{\text{BS-sur}}$, conditioned on $\mathbf{g}_{\text{relay-UE},u}$. Since linear transformations of Gaussian random matrices remain Gaussian, \mathbf{T}_u is a zero-mean complex Gaussian vector. Its covariance is followed by applying the identity $\mathbb{E}\{\mathbf{G}^H \mathbf{B} \mathbf{G}\} = \text{tr}(\mathbf{B}) \mathbf{I}$ for Gaussian matrices with i.i.d. entries and then averaging over $\mathbf{g}_{\text{relay-UE},u}$, which yields (18) and therefore completes the proof. ■

Additionally, since \mathbf{w} is isotropic and independent of \mathbf{T}_u , the scalar projection $h_u^{\text{sw}} = \mathbf{T}_u \mathbf{w}$ is thus distributed as

$$h_u^{\text{sw}} \sim \mathcal{CN}(0, \Omega_{\text{sw},u}). \quad (19)$$

D. Direct Path Contribution

From (9), the effective direct link is given by

$$h_u^{\text{dl,eff}} = \mathbf{h}_u^{\text{dl}} \mathbf{w} = \sqrt{\beta_{\text{DL},u}} \mathbf{g}_u^{\text{dl}} \mathbf{w}. \quad (20)$$

Because \mathbf{g}_u^{dl} has independent $\mathcal{CN}(0, 1)$ components and \mathbf{w} is a unit-norm vector independent of it, the projection $\mathbf{g}_u^{\text{dl}} \mathbf{w}$ remains $\mathcal{CN}(0, 1)$; this follows from the rotational invariance of complex Gaussian vectors. Hence, we have

$$h_u^{\text{dl,eff}} \sim \mathcal{CN}(0, \beta_{\text{DL},u}). \quad (21)$$

E. Distribution of the Equivalent Channel

Since h_u^{sw} and $h_u^{\text{dl,eff}}$ are independent zero-mean complex Gaussian random variables, their sum in (14) is also Gaussian. This leads to the following fundamental result.

Theorem 1 (Equivalent Channel Distribution). *The effective single-user channel $h_u^{\text{eq}} = h_u^{\text{sw}} + h_u^{\text{dl,eff}}$ is distributed as*

$$h_u^{\text{eq}} \sim \mathcal{CN}(0, \Omega_{\text{eq},u}), \quad (22)$$

where we have

$$\Omega_{\text{eq},u} = \Omega_{\text{sw},u} + \beta_{\text{DL},u}, \quad (23)$$

and accordingly, the channel's power gain $|h_u^{\text{eq}}|^2$ is exponential with mean $\Omega_{\text{eq},u}$.

Proof: The surface wave-assisted component h_u^{sw} and the direct component $h_u^{\text{dl,eff}}$ are independent zero-mean complex Gaussian random variables with variances $\Omega_{\text{sw},u}$ and $\beta_{\text{DL},u}$, respectively. Since the sum of independent complex Gaussian random variables remains complex Gaussian with variance equal to the sum of the individual variances, h_u^{eq} follows $\mathcal{CN}(0, \Omega_{\text{eq},u})$, where $\Omega_{\text{eq},u} = \Omega_{\text{sw},u} + \beta_{\text{DL},u}$. ■

IV. SINGLE-USER PERFORMANCE

We here consider the single-user case, where the received signal depends solely on the composite scalar channel $h \equiv h_u^{\text{eq}}$. For notational simplicity, the user index is omitted. The channel h is circularly symmetric complex Gaussian with variance Ω_{eq} , incorporating both the surface wave-assisted gain and any residual direct propagation. This section establishes closed-form expressions for the outage probability and ergodic capacity under this composite fading model.

A. Effective SNR

With a single intended stream and transmit power P , the received signal reduces to

$$y = \sqrt{P} h x + z_{\text{relay}} + n, \quad (24)$$

where x is a unit-power symbol, $n \sim \mathcal{CN}(0, \sigma^2)$ is the receiver noise, and z_{relay} is the noise introduced by the launcher/relay subsystem. Conditioned on the launcher-to-UE channel, the relay-induced noise power equals

$$\mathbb{E}\{|z_{\text{relay}}|^2 \mid \mathbf{h}_{\text{relay-UE}}\} = \sigma_r^2 \|\mathbf{h}_{\text{relay-UE}} \mathbf{W}_{\text{relay}}\|^2. \quad (25)$$

Averaging over the Rayleigh fading distribution of $\mathbf{h}_{\text{relay-UE}}$, and using standard trace identities for Gaussian vectors, we define the effective noise variance as

$$\sigma_{\text{eff}}^2 = \sigma^2 + \sigma_r^2 \beta_{\text{LU}} \text{tr}(\mathbf{W}_{\text{relay}} \mathbf{W}_{\text{relay}}^H), \quad (26)$$

where β_{LU} is the large-scale gain of the launcher-to-UE hop. The resultant instantaneous SNR is therefore

$$\gamma = \frac{P|h|^2}{\sigma_{\text{eff}}^2} = \rho |h|^2, \quad (27)$$

with the effective SNR given by

$$\rho = \frac{P}{\sigma_{\text{eff}}^2}. \quad (28)$$

B. Outage Probability

Let R_0 represent the target spectral efficiency in bits per second per Hertz (bps/Hz). An outage occurs whenever the instantaneous mutual information $\log_2(1 + \gamma)$ falls below R_0 . Because h is zero-mean complex Gaussian with variance Ω_{eq} , the magnitude square $|h|^2$ is exponential with mean Ω_{eq} , which directly enables a closed-form expression.

Theorem 2 (Outage Probability). *Let $h \sim \mathcal{CN}(0, \Omega_{\text{eq}})$ and $\gamma = \rho |h|^2$. For any target rate $R_0 > 0$, the outage probability is formulated as*

$$P_{\text{out}}(R_0) = 1 - \exp\left(-\frac{\gamma_0}{\rho \Omega_{\text{eq}}}\right), \quad (29)$$

where $\gamma_0 = 2^{R_0} - 1$.

Proof: The outage event is equivalent to $\gamma < \gamma_0$, and thus

$$P_{\text{out}}(R_0) = \Pr\{\gamma < \gamma_0\} = \Pr\left\{|h|^2 < \frac{\gamma_0}{\rho}\right\}. \quad (30)$$

Since $|h|^2$ is exponential with mean Ω_{eq} , its cumulative density function (CDF) is expressed as

$$F_{|h|^2}(x) = 1 - \exp\left(-\frac{x}{\Omega_{\text{eq}}}\right), \quad x \geq 0, \quad (31)$$

which, when evaluated at $x = \gamma_0/\rho$, yields (29). ■

It is worth pointing out that the influence of the E-FAS environment is characterized by entirely the parameter Ω_{eq} , which encapsulates the deterministic surface wave propagation effects and any remaining direct path component.

C. Ergodic Capacity

The ergodic capacity is defined as

$$C = \mathbb{E}\{\log_2(1 + \gamma)\} = \mathbb{E}\{\log_2(1 + \rho |h|^2)\}. \quad (32)$$

Given that $|h|^2$ is exponentially distributed, the integral admits a well-known closed form.

Theorem 3 (Ergodic Capacity). *For $h \sim \mathcal{CN}(0, \Omega_{\text{eq}})$ and $\gamma = \rho |h|^2$, the ergodic capacity of the single-user E-FAS considered is obtained as*

$$C = \frac{1}{\ln 2} \exp\left(\frac{1}{\rho \Omega_{\text{eq}}}\right) \text{E}_1\left(\frac{1}{\rho \Omega_{\text{eq}}}\right), \quad (33)$$

where $E_1(\cdot)$ denotes the exponential integral of

$$E_1(x) = \int_x^\infty \frac{e^{-t}}{t} dt, \quad x > 0. \quad (34)$$

Proof: Since the SNR γ follows the exponential distribution, the corresponding probability density function (PDF) is written as

$$f_\gamma(x) = \frac{1}{\rho\Omega_{\text{eq}}} \exp\left(-\frac{x}{\rho\Omega_{\text{eq}}}\right), \quad x \geq 0. \quad (35)$$

Thus, we have

$$C = \frac{1}{\rho\Omega_{\text{eq}} \ln 2} \int_0^\infty \ln(1+x) \exp\left(-\frac{x}{\rho\Omega_{\text{eq}}}\right) dx. \quad (36)$$

Applying the standard identity of

$$\int_0^\infty \ln(1+x) e^{-ax} dx = \frac{1}{a} e^a E_1(a), \quad a > 0, \quad (37)$$

associated with $a = 1/(\rho\Omega_{\text{eq}})$ yields (33). \blacksquare

D. High-SNR Asymptotics

The behavior at high SNR provides insight into both the diversity order and coding gain. As $\rho \rightarrow \infty$, $1/(\rho\Omega_{\text{eq}}) \rightarrow 0$, and the exponential integral admits the approximation

$$E_1(x) = -\gamma_E - \ln(x) + x + o(x), \quad (38)$$

where γ_E is Euler's constant. Substituting into (33) yields

$$C \approx \frac{1}{\ln 2} \left[-\gamma_E - \ln\left(\frac{1}{\rho\Omega_{\text{eq}}}\right) \right] = \log_2(\rho\Omega_{\text{eq}}) - \frac{\gamma_E}{\ln 2}. \quad (39)$$

The pre-log factor equals one, confirming that the diversity order is unity, as expected for a single channel. The parameter Ω_{eq} appears multiplicatively inside the logarithm, indicating that improvements in surface wave-guided gain through enhanced routing, optimized launcher placement, or reduced attenuation translate directly into additional coding gain.

V. MULTIUSER E-FAS USING ZF PRECODING

In this section, we extend our analysis to the multiuser downlink ($K \geq 1$) and investigate the performance of ZF precoding at the BS based on the equivalent BS-UE channel matrix derived from the E-FAS-assisted propagation.

A. Equivalent Channel Matrix

For UE u , the end-to-end channel operating from the BS, combining both the surface wave-guided and direct components, can be represented by an $M \times 1$ vector \mathbf{h}_u^{eq} . Motivated by the single-user analysis and leveraging Lemma 1, we model \mathbf{h}_u^{eq} as a complex Gaussian vector having independent entries and UE-dependent variance, i.e.,

$$\mathbf{h}_u^{\text{eq}} \sim \mathcal{CN}(\mathbf{0}, \Omega_{\text{eq},u} \mathbf{I}_M). \quad (40)$$

Equation (40) follows from the linearity of the end-to-end channel model and the fact that deterministic surface wave routing preserves Gaussianity of the underlying space wave

components. Stacking the channels to all K UEs yields the equivalent channel matrix

$$\mathbf{H}_{\text{eq}} = [\mathbf{h}_1^{\text{eq}}, \dots, \mathbf{h}_K^{\text{eq}}] \in \mathbb{C}^{M \times K}, \quad (41)$$

whose columns are mutually independent but not necessarily identically distributed, since the large-scale parameters $\Omega_{\text{eq},u}$ may differ across the UEs.

To obtain tractable closed-form expressions and highlight the fundamental impact of E-FAS, we assume the symmetric case,² where all UEs experience the same effective E-FAS-assisted variance, i.e., $\Omega_{\text{eq},u} = \Omega_{\text{eq}}$ for all u . Under this assumption, the entries of \mathbf{H}_{eq} are i.i.d. $\mathcal{CN}(0, \Omega_{\text{eq}})$, and the multiuser channel reduces to the classical Rayleigh MU-MIMO model, scaled by the E-FAS-induced factor Ω_{eq} .

B. ZF Precoding and Per-User SNR

Let the total BS transmit power denote P , equally allocated among the K UEs so that $P_u = P/K$. With ZF precoding, the BS employs a precoder matrix

$$\mathbf{W} = [\mathbf{w}_1, \dots, \mathbf{w}_K] = \mathbf{H}_{\text{eq}} (\mathbf{H}_{\text{eq}}^H \mathbf{H}_{\text{eq}})^{-1} \mathbf{D}, \quad (42)$$

where the diagonal matrix \mathbf{D} is chosen to satisfy a desired power normalization. Specifically, in this work, we focus on column-normalized ZF precoding, where each precoding vector satisfies $\|\mathbf{w}_u\|^2 = 1$. In the ideal ZF regime, the multiuser interference is perfectly cancelled, and the signal received at UE u reduces to

$$y_u = \sqrt{P_u} \mathbf{h}_u^{\text{eq},H} \mathbf{w}_u x_u + z_{u,\text{relay}} + n_u, \quad (43)$$

so that the instantaneous post-ZF SNR is

$$\gamma_u^{\text{ZF}} = \frac{P_u |\mathbf{h}_u^{\text{eq},H} \mathbf{w}_u|^2}{\sigma_{\text{eff}}^2}. \quad (44)$$

It is useful to express (44) in terms of the Gram matrix

$$\mathbf{G} = \mathbf{H}_{\text{eq}}^H \mathbf{H}_{\text{eq}} \in \mathbb{C}^{K \times K}. \quad (45)$$

Under conventional ZF with column normalization, and for i.i.d. Rayleigh fading with variance Ω_{eq} , the post-ZF SNR can be written in distribution as

$$\gamma_u^{\text{ZF}} \stackrel{d}{=} \frac{P/K}{\sigma_{\text{eff}}^2} \frac{1}{[(\mathbf{G}/\Omega_{\text{eq}})^{-1}]_{u,u}}. \quad (46)$$

Theorem 4 (ZF SNR Distribution). *Under an isotropic precoder, with $M \geq K$ and equal power allocation, the per-user ZF SNR γ_u^{ZF} is gamma-distributed with PDF*

$$f_{\gamma_u^{\text{ZF}}}(x) = \frac{1}{\Gamma(m)\theta^m} x^{m-1} e^{-x/\theta}, \quad x \geq 0, \quad (47)$$

where the shape parameter is $m = M - K + 1$ and the scale parameter is given by

$$\theta = \frac{P}{K\sigma_{\text{eff}}^2} \Omega_{\text{eq}}. \quad (48)$$

Proof: For an $M \times K$ matrix with i.i.d. $\mathcal{CN}(0, \Omega_{\text{eq}})$ entries and column-normalized ZF precoding, the post-ZF SNR of

²While the analysis focuses on the symmetric case for analytical clarity, the derived framework directly extends to asymmetric user scenarios with user-dependent variances $\Omega_{\text{eq},u}$, at the expense of more involved expressions.

each UE is proportional to the inverse of a diagonal element of $(\mathbf{H}_{\text{eq}}^H \mathbf{H}_{\text{eq}})^{-1}$. It is well known that the reciprocal of this quantity follows a chi-squared distribution with $2(M - K + 1)$ DoF, which corresponds to a gamma distribution with shape parameter $M - K + 1$. The scale parameter is determined by the per-user transmit power P/K , the effective noise variance σ_{eff}^2 , and the channel variance Ω_{eq} . As a result, the stated result is obtained and the proof is complete. ■

C. ZF Ergodic Sum-Rate

The ergodic sum-rate under ZF precoding is given by

$$R_{\text{sum}}^{\text{ZF}} = \sum_{u=1}^K \mathbb{E} \{ \log_2 (1 + \gamma_u^{\text{ZF}}) \}. \quad (49)$$

In the symmetric case, all UEs share the same distribution, and the expression simplifies to

$$R_{\text{sum}}^{\text{ZF}} = K \mathbb{E} \{ \log_2 (1 + \gamma^{\text{ZF}}) \}, \quad (50)$$

where γ^{ZF} denotes a generic random gamma variable having the PDF given above.

A closed-form expression for $R_{\text{sum}}^{\text{ZF}}$ in elementary functions is in general not available for this expectation. However, an accurate and insightful approximation in the moderate-to-high SNR regime replaces the random SNR by its mean. Since

$$\mathbb{E} \{ \gamma^{\text{ZF}} \} = m\theta = (M - K + 1) \frac{P}{K\sigma_{\text{eff}}^2} \Omega_{\text{eq}}, \quad (51)$$

the ergodic sum-rate can be approximated as

$$R_{\text{sum}}^{\text{ZF}} \approx K \log_2 \left(1 + (M - K + 1) \frac{P}{K\sigma_{\text{eff}}^2} \Omega_{\text{eq}} \right). \quad (52)$$

This approximation is accurate in the moderate-to-high SNR regime and when the number of BS antennas exceeds the number of UEs, as confirmed by the results in Section VI.

The expression in (52) reveals that the impact of E-FAS on the multiuser sum-rate is captured entirely through the effective channel variance Ω_{eq} , which reflects the surface wave-assisted gain and cylindrical path-loss behavior. For a fixed Ω_{eq} and sufficiently large antenna surplus $M - K$, the sum-rate scales approximately linearly with K at high SNR, consistent with classical ZF-based MU-MIMO systems. More refined approximations can be obtained by integrating the gamma density against $\log_2(1 + x)$ but such refinements do not alter the fundamental scaling behavior highlighted by (52).

VI. NUMERICAL RESULTS

In this section, we evaluate the performance of the proposed E-FAS-assisted wireless system through Monte-Carlo simulations and compare the results with the analytical expressions derived. Unless otherwise stated, the system parameters are set as $M = 16$, $K = 4$, $\text{SNR} = 10$ dB, and $R_0 = 1$ bps/Hz. The equivalent end-to-end channel variance is modeled as $\Omega_{\text{eq}} = \beta_{\text{DL}} + \Omega_{\text{sw}}$, where $\beta_{\text{DL}} = 0.01$ denotes the large-scale gain of the direct BS-UE link and $\Omega_{\text{sw}} \in \{1, 5, 10\}$ represents the surface wave-assisted gain provided by E-FAS. The benchmark operating without E-FAS corresponds to direct transmission only, i.e., $\Omega_{\text{sw}} = 0$, so that $\Omega_{\text{eq}} = \beta_{\text{DL}}$. Equal

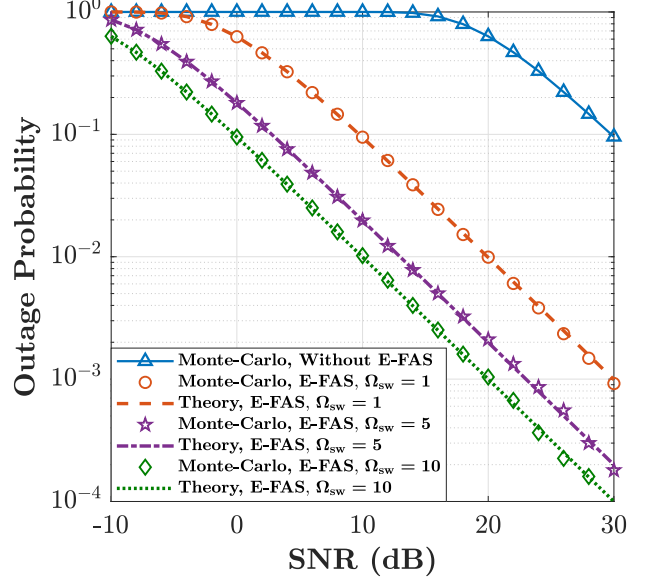


Fig. 2. Single-user outage probability versus SNR with different surface wave gains Ω_{sw} .

power allocation among UEs is assumed for all multiuser transmissions and the noise variance is normalized to unity. Additionally, for multiuser transmission, ZF precoding with column normalization is employed.

Fig. 2 depicts the single-user outage probability as a function of the SNR for the baseline system without E-FAS and for E-FAS-assisted transmission with different surface wave gains Ω_{sw} . We see that for all considered values of Ω_{sw} , the analytical outage expressions closely match the simulations over the entire SNR range, validating the accuracy of the derived closed-form outage probability. The benchmark case without E-FAS exhibits a significantly higher outage probability, particularly in the moderate-to-high SNR regime. This behavior is attributed to the weak direct BS-UE link, characterized by the small large-scale gain β_{DL} , which severely limits link reliability even at high transmit powers. In contrast, E-FAS leads to a pronounced improvement in outage performance. As Ω_{sw} increases, the outage curves shift markedly to the left, indicating substantial SNR gains at a given outage level. This improvement stems from the additional surface wave-assisted propagation path, which enhances the effective channel variance Ω_{eq} and mitigates the detrimental effects of blockage and path loss associated with the direct link. Moreover, the approximately parallel slopes of the outage curves in the high-SNR regime indicate that E-FAS primarily provides a power gain rather than an increase in diversity order, which remains unity for single-user transmission.

Fig. 3 illustrates the ergodic capacity of the single-user downlink in terms of the SNR for different surface wave gains Ω_{sw} . It is seen that the baseline system operating without E-FAS achieves a very limited capacity, especially in the low- and moderate-SNR regimes, due to the weak direct BS-UE link characterized by the small large-scale gain β_{DL} . By contrast, the incorporation of E-FAS yields a substantial capacity en-

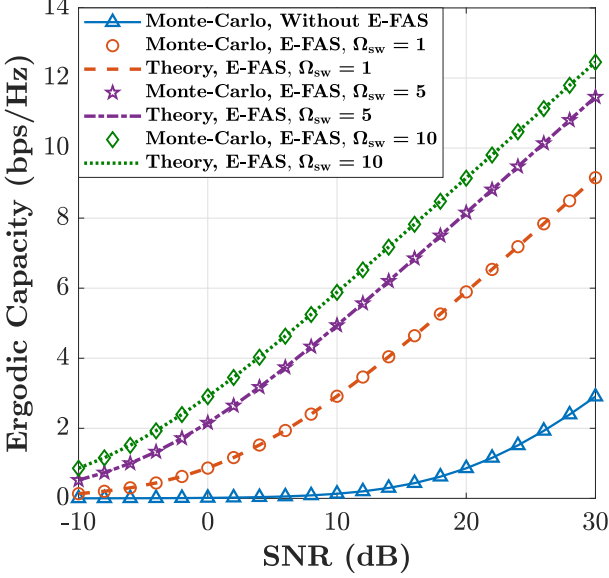


Fig. 3. Single-user ergodic capacity versus SNR with different surface wave gains Ω_{sw} .

hancement across the entire SNR range. Moreover, increasing the surface wave gain Ω_{sw} leads to a nearly uniform upward shift of the capacity curves, indicating that E-FAS primarily improves the effective channel strength rather than altering the fundamental scaling behavior with SNR. In the high-SNR regime, the capacity grows approximately logarithmically with SNR, as expected, with the E-FAS-induced gain appearing as an additive offset in the capacity expression. Therefore, these results demonstrate that E-FAS can significantly enhance spectral efficiency by compensating for severe path loss and blockage in the direct transmission link.

Fig. 4 illustrates the statistical characterization of the per-user ZF SINR in the E-FAS-assisted multiuser downlink, in which Fig. 4(a) illustrates the PDF and Fig. 4(b) depicts the corresponding CDF. The Monte-Carlo simulation results are compared with the analytical approximation derived based on the gamma distribution. It is observed that the analytical curves closely follow the simulation results for both the PDF and the CDF, demonstrating an excellent agreement across the entire range of SINR values. This confirms the accuracy of the distribution derived for the per-user ZF SINR under the E-FAS-assisted equivalent channel model assumed and validates the use of the gamma approximation for performance analysis. Furthermore, the unimodal shape of the PDF in Fig. 4(a) reflects the concentration of the ZF SINR around its mean value, while the smooth and steep transition of the CDF in Fig. 4(b) indicates relatively low variability in the post-ZF SINR. These characteristics are consistent with the behavior of ZF precoding in systems with a sufficient antenna surplus at the BS. Consequently, the results in Fig. 4 provide strong evidence that the proposed analytical framework accurately captures the key statistical properties of the ZF SINR in E-FAS-assisted multiuser transmission.

Fig. 5 illustrates the ZF sum-rate of the multiuser downlink

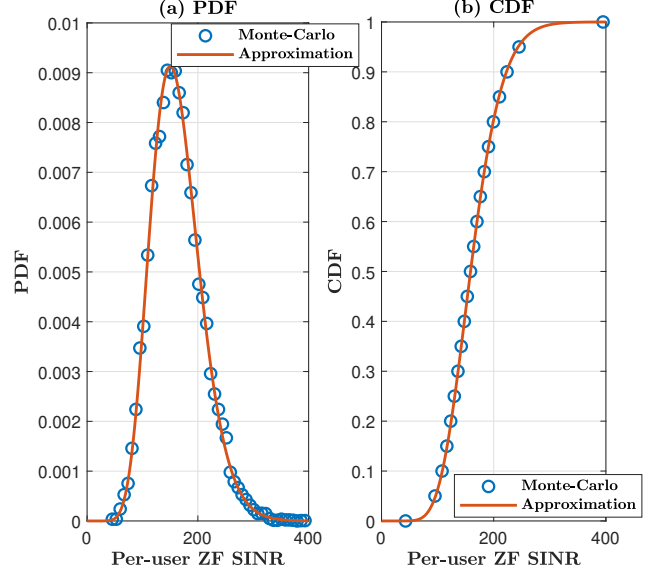


Fig. 4. Statistical characterization of the per-user ZF SINR in the E-FAS-assisted multiuser downlink: (a) PDF and (b) CDF.

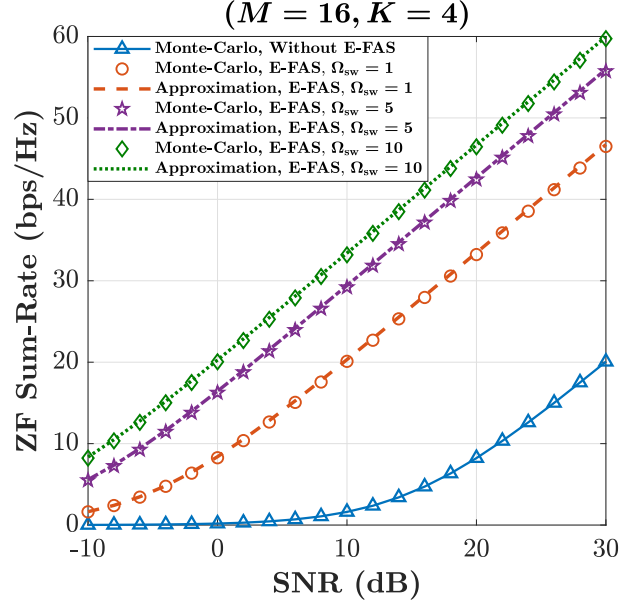


Fig. 5. ZF sum-rate versus SNR for the multiuser downlink with $M = 16$ and $K = 4$, with different surface wave gains Ω_{sw} .

as a function of the SNR for $M = 16$ and $K = 4$, under different surface wave gains Ω_{sw} . The analytical approximation is seen to closely match the Monte-Carlo simulation results over the entire SNR range, validating the accuracy of the proposed mean-SINR-based characterization. For a fixed number of UEs, increasing Ω_{sw} results in an almost uniform upward shift of the sum-rate curves, indicating that E-FAS enhances the effective channel quality experienced after ZF processing without altering the underlying ZF scaling behavior.

Fig. 6 represents the ZF sum-rate in terms of the number of UEs K for a fixed number of BS antennas $M = 16$ and a

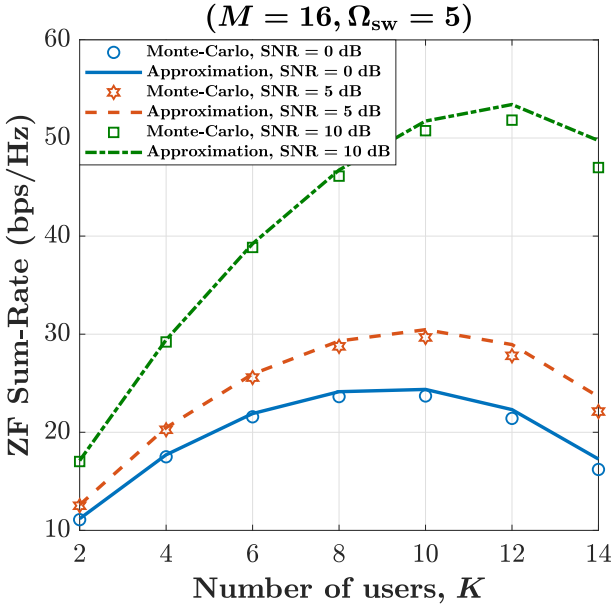


Fig. 6. ZF sum-rate versus the number of UEs K for $M = 16$ and $\Omega_{\text{sw}} = 5$, under different SNR values.

fixed surface wave gain $\Omega_{\text{sw}} = 5$, under different SNR levels. The figure demonstrates a clear trade-off between spatial multiplexing and inter-user interference suppression under ZF precoding. For each SNR value, the sum-rate initially increases with K due to the multiplexing gain offered by serving more UEs. However, beyond a certain point, further increasing K leads to a reduction in the sum-rate, as the effective post-ZF SINR degrades when the number of UEs approaches the available spatial DoF at the BS. This behavior highlights the fundamental limitation imposed by the finite antenna array size. Additionally, the optimal operating point in terms of the number of UEs increases with SNR, indicating that higher SNRs can support more aggressive spatial multiplexing.

Fig. 7 depicts the ZF sum-rate versus the number of UEs K at a fixed SNR of 5 dB and $\Omega_{\text{sw}} = 5$, for different numbers of BS antennas M . The figure highlights the beneficial impact of antenna resources on the user-loading behavior. It is observed that increasing M yields a consistent improvement in sum-rate across the entire range of K , and, importantly, delays the onset of the rate degradation at high user loads. This is because a larger antenna array provides additional spatial DoF, increasing $M - K + 1$ and thereby strengthening the post-ZF SINR for each UE. Consequently, systems with larger M can support more UEs before the ZF penalty becomes dominant. The analytical approximation tracks the Monte-Carlo simulation results closely, confirming that the proposed framework captures the dependence of the ZF sum-rate on both the UE loading K and the antenna surplus $M - K$.

VII. CONCLUSION

A tractable performance analysis for E-FAS-assisted MU-MIMO downlink transmission was developed and presented. By combining physics-based surface wave propagation with conventional small-scale fading on the space wave segments, we showed that the resultant end-to-end BS-UE channel admits

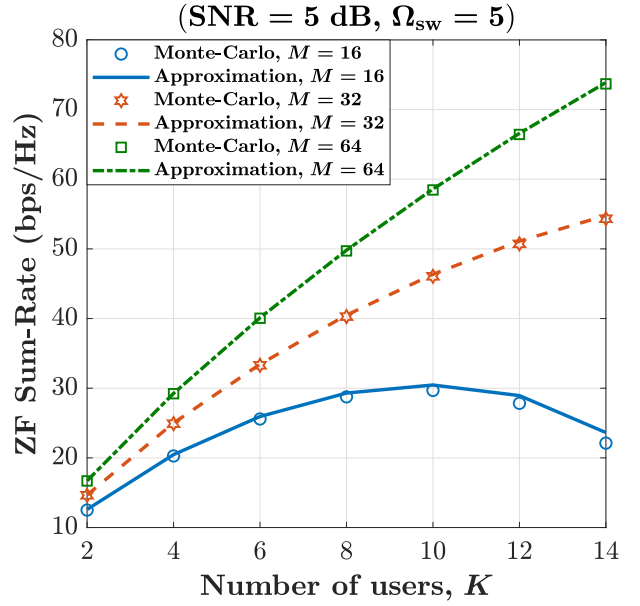


Fig. 7. ZF sum-rate versus the number of UEs K at SNR = 5 dB and $\Omega_{\text{sw}} = 5$, for different numbers of BS antennas M .

a compact equivalent representation. In particular, we revealed that despite the layered propagation structure of E-FAS, the effective channel remains complex Gaussian, with an average power that captures the surface wave-assisted gain and the reduced attenuation associated with quasi-two-dimensional (2D) propagation. Building on this result, closed-form expressions were derived for the outage probability and ergodic capacity for the single-user case, together with asymptotic characterizations that demonstrate how E-FAS improves the coding gain, while preserving the fundamental diversity order. For the multiuser scenario, the post-processing SINR under ZF precoding was characterized, leading to accurate approximations of the ergodic sum-rate that reveal the joint impact of E-FAS-induced channel enhancement and spatial DoF at the BS. Monte-Carlo simulations were shown to closely match the analytical results across a wide range of system parameters, thereby validating the proposed framework. Therefore, the analysis developed bridges the gap between EM-level E-FAS modeling and classical information-theoretic performance metrics, enabling fair and physically meaningful benchmarking against conventional space wave and RIS-based architectures.

REFERENCES

- [1] F. Tariq *et al.*, “A speculative study on 6G,” *IEEE Wireless Commun.*, vol. 27, no. 4, pp. 118–125, Aug. 2020.
- [2] W. Jiang, B. Han, M. A. Habibi and H. D. Schotten, “The road towards 6G: A comprehensive survey,” *IEEE Open J. Commun. Soc.*, vol. 2, pp. 334–366, Feb. 2021.
- [3] C.-X. Wang *et al.*, “On the road to 6G: Visions, requirements, key technologies, and testbeds,” *IEEE Commun. Surv. & Tut.*, vol. 25, no. 2, pp. 905–974, 2nd Quart. 2023.
- [4] D. A. U. Villalonga, H. OdetAlla, M. J. Fernández-Getino García, and A. Flizikowski, “Spectral efficiency of precoded 5G-NR in single and multi-user scenarios under imperfect channel knowledge: A comprehensive guide for implementation,” *Electronics*, vol. 11, no. 24, p. 4237, Dec. 2022.

[5] G. J. Foschini, "Layered space-time architecture for wireless communication in a fading environment when using multi-element antennas," *Bell Labs Tech. J.*, vol. 1, no. 2, pp. 41–59, Autumn 1996.

[6] E. Telatar, "Capacity of multi-antenna Gaussian channels," *Euro. Trans. Telecommun.*, vol. 10, no. 6, pp. 585–595, 1999.

[7] K. K. Wong, R. D. Murch, R. S.-K. Cheng and K. B. Letaief, "Optimizing the spectral efficiency of multiuser MIMO smart antenna systems," in *Proc. IEEE Wirel. Commun. Netw. Conf. (WCNC)*, vol. 1, pp. 426–430, 23–28 Sept. 2000, Chicago, IL, USA.

[8] K. K. Wong, R. D. Murch and K. B. Letaief, "Performance enhancement of multiuser MIMO wireless communication systems," *IEEE Trans. Commun.*, vol. 50, no. 12, pp. 1960–1970, Dec. 2002.

[9] K. K. Wong, R. D. Murch, and K. Ben Letaief, "A joint-channel diagonalization for multiuser MIMO antenna systems," *IEEE Trans. Wireless Commun.*, vol. 4, no. 2, pp. 773–786, Jul. 2003.

[10] S. Vishwanath, N. Jindal and A. Goldsmith, "Duality, achievable rates, and sum-rate capacity of Gaussian MIMO broadcast channels," *IEEE Trans. Inf. Theory*, vol. 49, no. 10, pp. 2658–2668, Oct. 2003.

[11] Q. H. Spencer, A. L. Swindlehurst and M. Haardt, "Zero-forcing methods for downlink spatial multiplexing in multiuser MIMO channels," *IEEE Trans. Sig. Process.*, vol. 52, no. 2, pp. 461–471, Feb. 2004.

[12] T. L. Marzetta, "Noncooperative cellular wireless with unlimited numbers of base station antennas," *IEEE Trans. Wireless Commun.*, vol. 9, no. 11, pp. 3590–3600, Nov. 2010.

[13] E. G. Larsson, O. Edfors, F. Tufvesson and T. L. Marzetta, "Massive MIMO for next generation wireless systems," *IEEE Commun. Mag.*, vol. 52, no. 2, pp. 186–195, Feb. 2014.

[14] Z. Wang *et al.*, "A tutorial on extremely large-scale MIMO for 6G: Fundamentals, signal processing, and applications," *IEEE Commun. Surv. & Tut.*, vol. 26, no. 3, pp. 1560–1605, thirdquarter 2024.

[15] T. S. Rappaport *et al.*, "Millimeter wave mobile communications for 5G cellular: It will work!," *IEEE Access*, vol. 1, pp. 335–349, 2013.

[16] A. F. Molisch, *Wireless communications*, John Wiley & Sons, vol. 34, 2012.

[17] R. W. Heath, N. González-Prelicic, S. Rangan, W. Roh and A. M. Sayeed, "An overview of signal processing techniques for millimeter wave MIMO systems," *IEEE J. Select. Topics Sig. Proc.*, vol. 10, no. 3, pp. 436–453, Apr. 2016.

[18] C. Liaskos *et al.*, "A new wireless communication paradigm through software-controlled metasurfaces," *IEEE Commun. Mag.*, vol. 56, no. 9, pp. 162–169, Sept. 2018.

[19] Jie Zhao *et al.*, "Programmable time-domain digital-coding metasurface for non-linear harmonic manipulation and new wireless communication systems," *National Sci. Review*, vol. 6, no. 2, pp. 231–238, Mar. 2019.

[20] C. Huang, A. Zappone, G. C. Alexandropoulos, M. Debbah, and C. Yuen, "Reconfigurable intelligent surfaces for energy efficiency in wireless communication," *IEEE Trans. Wireless Commun.*, vol. 18, no. 8, pp. 4157–4170, Aug. 2019.

[21] E. Basar *et al.*, "Wireless communications through reconfigurable intelligent surfaces," *IEEE Access*, vol. 7, pp. 116753–116773, 2019.

[22] X. Mu, Y. Liu, L. Guo, J. Lin and R. Schober, "Simultaneously transmitting and reflecting (STAR) RIS aided wireless communications," *IEEE Trans. Wireless Commun.*, vol. 21, no. 5, pp. 3083–3098, May 2022.

[23] J. An, C. Xu, L. Gan and L. Hanzo, "Low-complexity channel estimation and passive beamforming for RIS-assisted MIMO systems relying on discrete phase shifts," *IEEE Trans. Commun.*, vol. 70, no. 2, pp. 1245–1260, Feb. 2022.

[24] J. T. Bernhard, *Reconfigurable antennas*, Synthesis Lectures on Antennas, 2007.

[25] B. Cetiner *et al.*, "Multifunctional reconfigurable MEMS integrated antennas for adaptive MIMO systems," *IEEE Commun. Mag.*, vol. 42, no. 12, pp. 62–70, Dec. 2004.

[26] K. K. Wong, A. Shojaeifard, K.-F. Tong, and Y. Zhang, "Fluid antenna systems," *IEEE Trans. Wireless Commun.*, vol. 20, no. 3, pp. 1950–1962, Mar. 2021.

[27] K. K. Wong, A. Shojaeifard, K.-F. Tong and Y. Zhang, "Performance limits of fluid antenna systems," *IEEE Commun. Lett.*, vol. 24, no. 11, pp. 2469–2472, Nov. 2020.

[28] W. K. New *et al.*, "A tutorial on fluid antenna system for 6G networks: Encompassing communication theory, optimization methods and hardware designs," *IEEE Commun. Surv. Tuts.*, vol. 27, no. 4, pp. 2325–2377, Aug. 2025.

[29] W.-J. Lu *et al.*, "Fluid antennas: Reshaping intrinsic properties for flexible radiation characteristics in intelligent wireless networks," *IEEE Commun. Mag.*, vol. 63, no. 5, pp. 40–45, May 2025.

[30] H. Hong *et al.*, "A contemporary survey on fluid antenna systems: Fundamentals and networking perspectives," *IEEE Trans. Netw. Sci. Eng.*, vol. 13, pp. 2305–2328, 2026.

[31] W. K. New *et al.*, "Fluid antenna systems: Redefining reconfigurable wireless communications," *IEEE J. Sel. Areas Commun.*, DOI:10.1109/JSAC.2025.3632097, 2026.

[32] T. Wu *et al.*, "Fluid antenna systems enabling 6G: Principles, applications, and research directions," to appear in *IEEE Wireless Commun.*, DOI:10.1109/MWC.2025.3629597, 2025.

[33] L. Zhu and K. K. Wong, "Historical review of fluid antenna and movable antenna," *arXiv preprint*, arXiv:2401.02362, 2024.

[34] Y. Shen *et al.*, "Design and experimental validation of mmWave surface wave enabled fluid antennas for future wireless communications," to appear in *IEEE Antennas & Wireless Propag. Lett.*, DOI:10.1109/LAWP.2026.3657059, 2026.

[35] R. Wang *et al.*, "Electromagnetically reconfigurable fluid antenna system for wireless communications: Design, modeling, algorithm, fabrication, and experiment," *IEEE J. Select. Areas Commun.*, DOI:10.1109/JSAC.2025.3625163, 2026.

[36] S. Zhang *et al.*, "Fluid antenna systems enabled by reconfigurable holographic surfaces: Beamforming design and experimental validation," *IEEE J. Select. Areas Commun.*, DOI:10.1109/JSAC.2025.3618797, 2026.

[37] B. Liu, K.-F. Tong, K. K. Wong, C.-B. Chae, and H. Wong, "Programmable meta-fluid antenna for spatial multiplexing in fast fluctuating radio channels," *Optics Express*, vol. 33, no. 13, pp. 28898–28915, 2025.

[38] B. Liu *et al.*, "Meta fluid antenna: Architecture design, performance analysis, experimental examination," *arXiv preprint*, arXiv:2509.12032, Sept. 2025.

[39] J. Zhang *et al.*, "A novel pixel-based reconfigurable antenna applied in fluid antenna systems with high switching speed," *IEEE Open J. Antennas & Propag.*, vol. 6, no. 1, pp. 212–228, Feb. 2025.

[40] B. Liu, T. Wu, K. K. Wong, H. Wong, and K. F. Tong, "Wideband pixel-based fluid antenna system: An antenna design for smart city," *IEEE Internet Things J.*, DOI:10.1109/JIOT.2025.3637319, 2025.

[41] K. K. Wong, C. Wang, S. Shen, C.-B. Chae and R. Murch, "Reconfigurable pixel antennas meet fluid antenna systems: A paradigm shift to electromagnetic signal and information processing," *IEEE Wireless Commun.*, DOI:10.1109/MWC.2025.3625130, 2026.

[42] K.-F. Tong, B. Liu, and K. K. Wong, "Designs and challenges in fluid antenna system hardware," *Electronics*, vol. 14, no. 7, p. 1458, 2025.

[43] M. Khammassi, A. Kamoun, and M.-S. Alouini, "A new analytical approximation of the fluid antenna system channel," *IEEE Trans. Wireless Commun.*, vol. 22, no. 12, pp. 8843–8858, Dec. 2023.

[44] F. R. Ghadi, K. K. Wong, F. J. López-Martínez, and K.-F. Tong, "Copula-based performance analysis for fluid antenna systems under arbitrary fading channels," *IEEE Commun. Lett.*, vol. 27, no. 10, pp. 2720–2724, Nov. 2023.

[45] W. K. New, K. K. Wong, H. Xu, K.-F. Tong, and C.-B. Chae, "Fluid antenna system: New insights on outage probability and diversity gain," *IEEE Trans. Wireless Commun.*, vol. 23, no. 5, pp. 4846–4859, Jan. 2024.

[46] P. Ramírez-Espinosa, D. Morales-Jimenez, and K. K. Wong, "A new spatial block-correlation model for fluid antenna systems," *IEEE Trans. Wireless Commun.*, vol. 23, no. 11, pp. 15829–15843, Nov. 2024.

[47] W. K. New, K. K. Wong, H. Xu, K.-F. Tong and C.-B. Chae, "An information-theoretic characterization of MIMO-FAS: Optimization, diversity-multiplexing tradeoff and q -outage capacity," *IEEE Trans. Wireless Commun.*, vol. 23, no. 6, pp. 5541–5556, Jun. 2024.

[48] C. Psomas, P. J. Smith, H. A. Suraweera and I. Krikidis, "Continuous fluid antenna systems: Modeling and analysis," *IEEE Commun. Lett.*, vol. 27, no. 12, pp. 3370–3374, Dec. 2023.

[49] H. Xu *et al.*, "Capacity maximization for FAS-assisted multiple access channels," *IEEE Trans. Commun.*, vol. 73, no. 7, pp. 4713–4731, Jul. 2025.

[50] Z. Cheng *et al.*, "Sum-rate maximization for fluid antenna enabled multiuser communications," *IEEE Commun. Lett.*, vol. 28, no. 5, pp. 1206–1210, May 2024.

[51] H. Xu *et al.*, "Channel estimation for FAS-assisted multiuser mmWave systems," *IEEE Commun. Lett.*, vol. 28, no. 3, pp. 632–636, Mar. 2024.

[52] H. Zhang *et al.*, "Learning-induced channel extrapolation for fluid antenna systems using asymmetric graph masked autoencoder," *IEEE Wireless Commun. Lett.*, vol. 13, no. 6, pp. 1665–1669, Jun. 2024.

[53] W. K. New *et al.*, "Channel estimation and reconstruction in fluid antenna system: Oversampling is essential," *IEEE Trans. Wireless Commun.*, vol. 24, no. 1, pp. 309–322, Jan. 2025.

[54] Z. Zhang, J. Zhu, L. Dai, and R. W. Heath Jr, "Successive Bayesian reconstructor for channel estimation in fluid antenna systems," *IEEE Trans. Wireless Commun.*, vol. 24, no. 3, pp. 1992–2006, Mar. 2025.

- [55] F. R. Ghadi *et al.*, "On performance of RIS-aided fluid antenna systems," *IEEE Wireless Commun. Lett.*, vol. 13, no. 8, pp. 2175–2179, Aug. 2024.
- [56] X. Lai *et al.*, "FAS-RIS: A block-correlation model analysis," *IEEE Trans. Veh. Technol.*, vol. 74, no. 2, pp. 3412–3417, Feb. 2025.
- [57] J. Yao *et al.*, "FAS-RIS communication: Model, analysis, and optimization," *IEEE Trans. Veh. Technol.*, vol. 74, no. 6, pp. 9938–9943, Jun. 2025.
- [58] A. Salem, K. K. Wong, G. Alexandropoulos, C.-B. Chae, and R. Murch, "A first look at the performance enhancement potential of fluid reconfigurable intelligent surface," *arXiv preprint*, [arXiv:2502.17116](https://arxiv.org/abs/2502.17116), 2025.
- [59] H. Xiao *et al.*, "Fluid reconfigurable intelligent surfaces: Joint on-off selection and beamforming with discrete phase shifts," *IEEE Wireless Commun. Lett.*, vol. 14, no. 10, pp. 3124–3128, Oct. 2025.
- [60] F. R. Ghadi *et al.*, "Performance analysis of wireless communication systems assisted by fluid reconfigurable intelligent surfaces," *IEEE Wireless Commun. Lett.*, vol. 14, no. 12, pp. 3922–3926, Dec. 2025.
- [61] H. Xiao *et al.*, "Fluid reconfigurable intelligent surface with element-Level pattern reconfigurability: Beamforming and pattern co-design," *IEEE Trans. Wireless Commun.*, vol. 25, pp. 10791–10806, 2026.
- [62] F. R. Ghadi *et al.*, "FIRES: Fluid integrated reflecting and emitting surfaces," *IEEE Wireless Commun. Lett.*, vol. 14, no. 11, pp. 3744–3748, Nov. 2025.
- [63] K. K. Wong, K.-F. Tong, Z. Chu and Y. Zhang, "A vision to smart radio environment: Surface wave communication superhighways," *IEEE Wireless Commun.*, vol. 28, no. 1, pp. 112–119, Feb. 2021.
- [64] H. Liu *et al.*, "Path loss and surface impedance models for surface wave-assisted wireless communication system," *IEEE Access*, vol. 12, pp. 125786–125799, Aug. 2024.
- [65] Z. Chu, K. F. Tong, K. K. Wong, C.-B. Chae, and C. H. Chan, "On propagation characteristics of reconfigurable surface wave platform: Simulation and experimental verification," *IEEE Access*, vol. 12, pp. 168744–168754, Nov. 2024.
- [66] Z. Chu *et al.*, "On propagation loss for reconfigurable surface wave communications," *IEEE Trans. Commun.*, vol. 73, no. 3, pp. 1547–1559, Mar. 2025.
- [67] K. K. Wong *et al.*, "Enormous fluid antenna systems (E-FAS): Rethinking the future of wireless communications," *Research Square preprint*, <https://doi.org/10.21203/rs.3.rs-8002084/v1>, 2025.
- [68] A. Shojaeifard *et al.*, "MIMO evolution beyond 5G through reconfigurable intelligent surfaces and fluid antenna systems," *Proc. IEEE*, vol. 110, no. 9, pp. 1244–1265, Sept. 2022.